INVITED ARTICLE

Piezoelectric polymer thin films with architected cuts

Lichen Fang
Department of Mechanical Engineering, Johns Hopkins University, Baltimore, Maryland 21218, USA; and Hopkins Extreme Materials Institute, Johns Hopkins University, Baltimore, Maryland 21218, USA

Jing Li
Department of Mechanical Engineering, Johns Hopkins University, Baltimore, Maryland 21218, USA; Hopkins Extreme Materials Institute, Johns Hopkins University, Baltimore, Maryland 21218, USA; and Hubei Key Laboratory of Advanced Technology for Automotive Components, Wuhan University of Technology, Wuhan, Hubei 430070, China

Zeyu Zhu, Santiago Orrego, and Sung Hoon Kang[a)]
Department of Mechanical Engineering, Johns Hopkins University, Baltimore, Maryland 21218, USA; and Hopkins Extreme Materials Institute, Johns Hopkins University, Baltimore, Maryland 21218, USA

(Received 29 September 2017; accepted 2 January 2018)

Introducing architected cuts is an attractive and simple approach to tune mechanical behaviors of planar materials like thin films for desirable or enhanced mechanical performance. However, little has been studied on the effects of architected cuts on functional materials like piezoelectric materials. We investigated how architected cut patterns affect mechanical and piezoelectric properties of polyvinylidene fluoride thin films by numerical, experimental, and analytical studies. Our results show that thin films with architected cuts can provide desired mechanical features like enhanced compliance, stretchability, and controllable Poisson's ratio and resonance frequency, while maintaining piezoelectric performance under static loadings. Moreover, we could observe maximum ~30% improvement in piezoelectric conversion efficiency under dynamic loadings and harvest energy from low frequency (<100 Hz) mechanical signals or low velocity (<5 m/s) winds, which are commonly existing in ambient environment. Using architected cuts doesn't require changing the material or overall dimensions, making it attractive for applications in self-powered devices with design constraints.

I. INTRODUCTION

In the past decades, there have been remarkable advances in designing, modeling, and fabricating architected materials,[1–11] which could achieve novel mechanical properties/behaviors by the interplay between materials and specially designed geometries.[12] In particular, due to readily available tools for shaping a diverse set of materials across different length scales, there have been many studies that investigated various planar periodic structures to introduce novel mechanical behaviors typically unavailable in bulk materials, including negative Poisson's ratio (auxetic),[13–17] stretchability,[18] trapping elastic energy,[19,20] negative effective swelling coefficient,[21] and controlling propagation of mechanical signals.[22–24] Among various approaches for making architected materials, introducing cuts ("kirigami") instead of large voids is a popular and straightforward approach to add architecture to thin films[18] and an attractive way to manipulate the properties of resulting architected materials with minimum effects on mechanical integrity compared to materials with large pores.[23] There have been studies demonstrating novel mechanical properties including enhanced conformability/stretchability,[18] negative Poisson's ratio,[25] enhanced fatigue life,[16] enhanced structure strength,[26] and controllable propagation of vibration,[23] using architected cuts.

Beyond materials used for load-bearing and/or energy dissipation, architected cuts could affect the properties of functional materials such as piezoelectric materials that convert mechanical energy into electrical energy and vice versa, which have been utilized for applications such as energy harvesting, sensing, actuation, and tissue regeneration.[27–29] In particular, piezoelectric materials have been actively studied for providing power to small and/or portable devices using dynamic mechanical energy from physical activities or ambient environment for applications including wearable sensors and self-powered devices,[30–33] which often require high compliance and/or stretchability. The mechanical energy from physical activities or environmental vibrations is typically at a low frequency range (<~100 Hz).[34] Therefore, we need to design and make devices suitable for this frequency range, which is often challenging due to constraints of material properties, geometries, and space limitations. Similar challenge exists in harvesting ambient wind energy using piezoelectric thin films for self-powered

Contributing Editor: Christopher Spadaccini
[a)]Address all correspondence to this author.
e-mail: shkang@jhu.edu
DOI: 10.1557/jmr.2018.6

devices, which gains lots of interest recently. Previous approaches tend to require high wind velocity (>5 m/s), which is not suitable for ambient wind that has a low wind velocity. Recently, it has been demonstrated that controlling a nondimensionalized bending stiffness [Eq. (1)] could be utilized to tune the range of the wind speed that can trigger flow-induced self-sustained flapping of piezoelectric materials for energy harvesting.[35] The previous study showed that the flapping of piezoelectric materials appears within the bending stiffness of $0.1 \leq K_B \leq 0.3$. So, as the wind speed decreases, we need to decrease the modulus or the thickness of the material or increase the length of the material. Nonetheless, this approach cannot be applied when there are limited available options for material properties and geometries due to design constraints.

$$K_B = \frac{Eh^3}{12(1-\nu^2)\rho_f U^2 L^3} \quad , \qquad (1)$$

(E: Young's modulus, h: thickness, ν: Poisson's ratio, L: length of the membrane, ρ_f: fluid density, and U: free-stream velocity.)

Introducing architected cuts can be potential solutions to address aforementioned challenges. Architected materials could be utilized to control the stress distribution within piezoelectric materials. For example, there have been interests in the effects of Poisson's ratio on piezoelectric outputs. It was proposed more than twenty years ago that auxetic materials could enhance electromechanical coupling.[36] Still, it was recently that numerical analysis predicted an auxetic planar piezoelectric cellular solid with hexagonal re-entrant geometry could have a combination of desirable properties (high piezo efficiency, low impedance, more extensibility, and sensitivity) which are absent in monolithic piezoelectric materials.[37] In addition, it was reported from the numerical analysis that multilayer structures comprising a planar auxetic substrate made of steel sandwiched between two piezoelectric layers showed enhanced power output compared to the case with a bulk middle substrate.[38] However, in this study, they did not consider auxetic structures made of piezoelectric materials. Rather, they studied the effects of the auxetic middle layer made of a nonpiezoelectric material on planar piezoelectric materials attached to the middle layer.

Introducing architected cuts into piezoelectric materials can tune not only their Poisson's ratios and potentially resulting functional properties but also other properties such as stretchability and resonance frequency, making it attractive for stretchable or flexible electronics and/or ambient energy harvesting. Intuitively, adding cuts could decrease rigidity, causing a decrease in resonance frequency providing a possible approach to harvest low frequency ambient energy and increase compliance and/or stretchability. In addition, introducing architected cut patterns can be a potential solution to tune the wind speed range that one can utilize with minimum effect on fluid–solid interactions due to very low porosity of the system.

So far, there is no systematic study about how the change of the architected cut patterns on piezoelectric materials affects their functions and mechanical behaviors. Here, we conducted parametric numerical and experimental studies combined with analytical modeling to investigate the effects of controlling cut patterns, in particular cut-out ratio on Poisson's ratio, static and dynamic piezoelectric performance, and compliance and stretchability. The results provide guides to select architected cut patterns for desirable mechanical and functional properties.

II. MATERIALS AND METHODS

A. Materials

We used commercially available metalized polyvinylidene fluoride (PVDF) piezo film sheets (Product #3-1003702-7, TE Connectivity, Berwyn, Pennsylvania) for this study. The film is poled along its thickness direction with metal electrodes on both surfaces. The electrode is made of 70 nm of copper covered with 10 nm of nickel, providing good conductivity and oxidation resistance. As the thickness of electrode is much smaller than the film thickness (0.11 mm), the electrodes could be considered having negligible contribution to the mechanical properties of the film.

B. Design

To tune the mechanical properties, including compliance, Poisson's ratio, and stretchability, we chose three desired cut patterns for this study based on findings from previous studies: unidirectional cut, square cut, and fractal cut. From definition and practices of kirigami, the removed materials should be of negligible amount. Especially, in experiments, the cut widths are always controlled to be much less than the length.[15,18,25,26,39,40] The unidirectional cut pattern has been investigated and applied in multiple studies, including graphene kirigami work.[40] The pattern with alternating cut distribution could increase the stretchability in one direction. The square cut was proposed by Grima et al.,[41] and the pattern was found to have tunable Poisson's ratio ranging from positive to negative by controlling the cut length. Recently, the fractal cut has been developed to introduce even higher stretchability compared to other cut patterns.[38] As we are interested in controlling the mechanical behaviors such as stretchability and Poisson's ratio by using architected cuts, we have decided to choose these three types of cut patterns (Fig. 1).

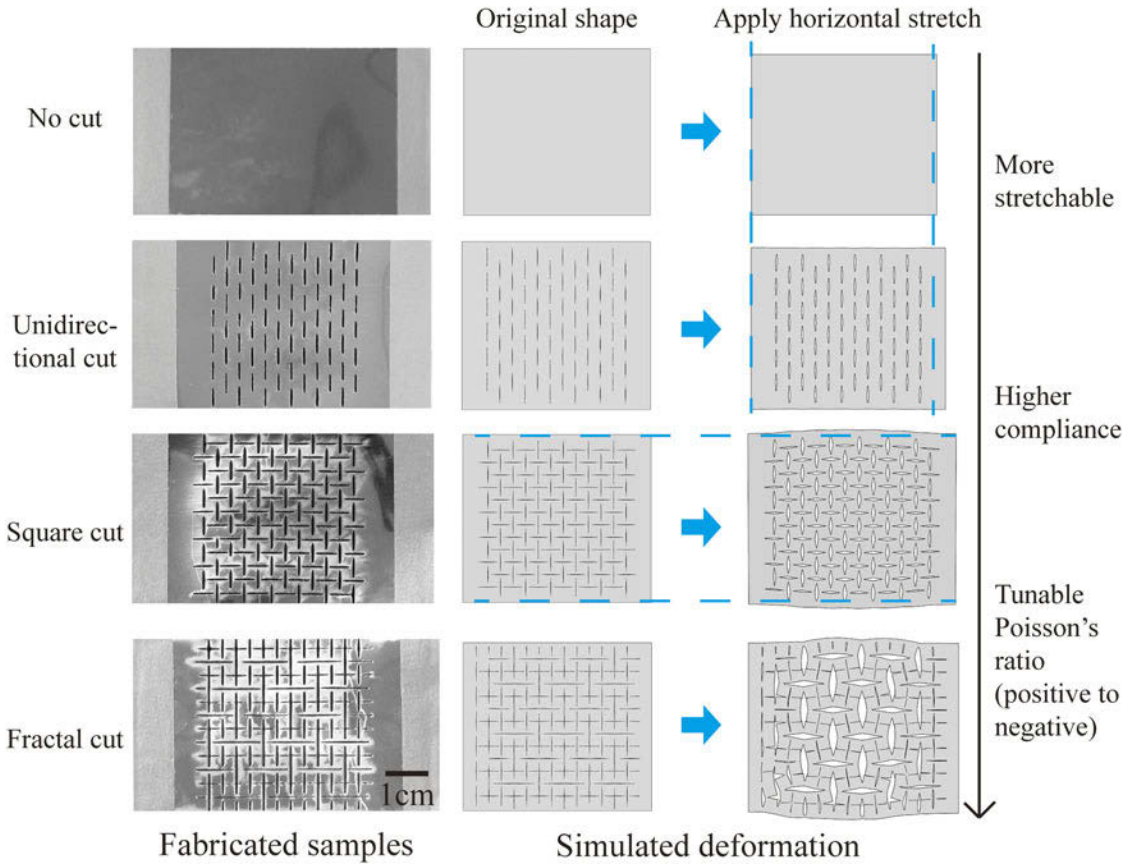

FIG. 1. Actual images and designs of specimens with different cut patterns.

C. Fabrication

We generated cut patterns on the PVDF piezoelectric film using a laser cutter (VLS6.60, Universal Laser Systems, Scottsdale, Arizona) with a cut width of ~0.2 mm (Fig. 1). The cutting patterns were drawn with SolidWorks (version 2016) and imported to the laser cutter. A laser intensity study was conducted to make sure that the cut was through while it was not too wide. After cutting, we verified that the cuts would not cause short-circuit between the top and bottom surfaces by measuring the resistance between two electrodes.

The cutting patterns were intentionally designed with insulation areas at both ends, leaving a 45 × 40.5 mm central area with cutting patterns, as shown in Fig. 2(a). This design allows us to add insulation tapes at the clamping areas to prevent external electrical signals. It can also mitigate the stress concentration at clamps to provide uniform stretch along the cut region. The samples were then attached with paper tapes to create insulation zones for mounting on mechanical loading equipment [see Fig. 2(b)]. Multiple samples with different cutting patterns [unidirectional, square, and fractal; Fig. 2(c)] and different cut-out ratios [0, 0.25, 0.50, and 0.75; Fig. 2(d)] were fabricated. Here, the cut-out ratio is defined as the cut length over the unit cell length, based on the geometries shown in Fig. 2(c), indicating how long the cuts occupy. When the cut-out ratio is 0, it means there is no cut while the ratio of 1 means the cut is long enough to connect each other, resulting in a complete cut along the whole surface.

As shown in Fig. 2(c), each sample is composed of m by n unit cells (in this study, we used $m = 6$ and $n = 6$). For fractal cut samples, the definition is slightly different due to the extra hierarchy. The unit cell is twice as large as others, and the first order cuts must be longer than half of the unit cell size to connect cuts of different hierarchies. Thus, in the case of the fractal cut, we defined the cut-out ratio by the length of second order cuts over unit cell length. Due to the different definition of the cut-out ratio, the measurement results of fractal cut samples may look a little different from others. If we consider the first order cut length, they naturally have cut-out ratios larger than 50%.

D. Simulations

We used the commercial finite element package Abaqus/Standard (version 6.13, Dassault Systèmes Americas Corp., Waltham, Massachusetts) to investigate

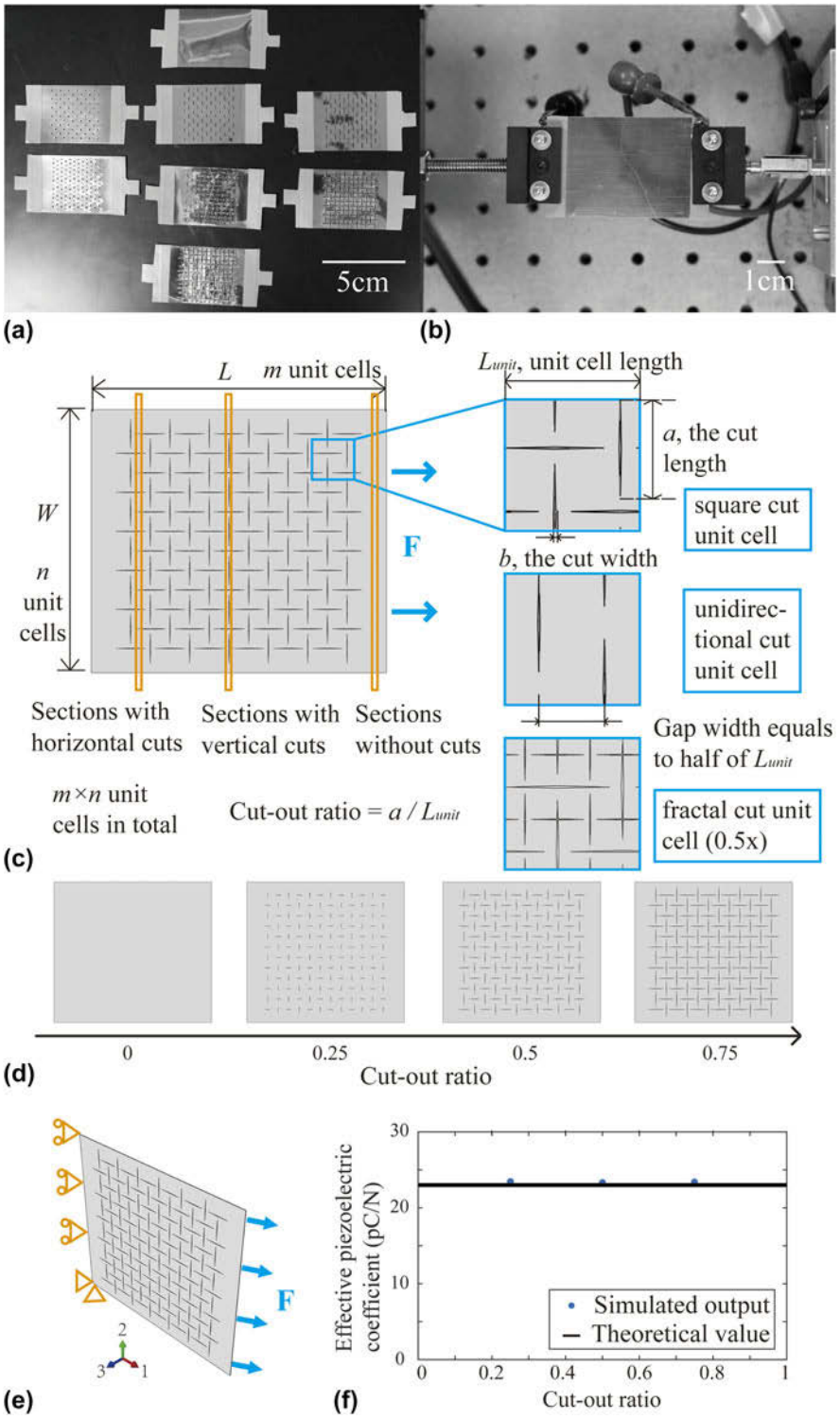

FIG. 2. (a) The laser cut samples with insulation tapes on both ends. (b) The uncut sample mounted on measurement setup. (c) The schematic of the system and the unit cells for different cut patterns. (d) The schematic of samples with different cut-out ratios. (e) The simulation setup showing that displacement boundary conditions were applied on one edge and force boundary condition on the other edge. (f) Effects of cut-out ratios on the effective piezoelectric coefficient of square cut patterns.

the effects of cut patterns. All static loading models share the same overall dimension, $45 \times 40.5 \times 0.11$ mm, while the inner architected cut structures are different. For dynamic loading models, the additional insulated clamping zone was accounted for calculating resonance frequency so that the length was increased to 50 mm to

match that of experiments. The left surface was constrained in one direction, while the bottom left corner point was fixed in all directions as well as set to be zero electric potential point [Fig. 2(e)]. Since we need to use the 3-1 mode (load in 1 direction, electric output in 3 direction) piezoelectricity, we built 3D finite element models with the 3D 8-node continuum linear piezoelectric brick element (Abaqus element type C3D8E). The mesh size was determined by the mesh convergence study to find the best element size for balancing accuracy and calculation cost [Fig. S1(a), see Supplementary Material S1 for details]. The model we used is the sample with unidirectional cut at 0.75 cut-out ratio. We tried different mesh sizes with the number of nodes changing from 28,000 to 400,000. From Fig. S1(a), we could see that the result converges at the node number equals to around 200,000. The mesh size is comparable to the sample's thickness, which means there would be a proper size mesh for the element. The material property was set to be elastic, with a Young's modulus of 1.5 GPa and a Poisson's ratio of 0.35 based on measurements. The dielectric coefficient was set as 110 pF/m and the piezoelectric coefficients were $d_{31} = 23$ pC/N, $d_{32} = 3$ pC/N, and $d_{33} = -33$ pC/N based on the data from the manufacturer.

In static piezoelectric simulation, for mechanical boundary conditions, we fixed one end and applied tensile force of 3.1 N (i.e., stress of 700 kPa) on the other side and left all other boundaries free. For the electrical boundary condition, we set the bottom left corner point (0, 0, 0) as the zero electric potential point. With this setup, we simulated multiple cut patterns with different cut-out ratios. We recorded the displacement and the electric potential of each unique node and processed them with MATLAB (see Supplementary Material S2 for details). The code found the elements at top and bottom surfaces, obtained the electric potential of those elements, and compared values between the two surfaces to give the electric potential difference in voltage. Based on the potential, we calculated the charge generation by multiplying capacitance. Then, we obtained the effective piezoelectric coefficient by dividing the generated charge with the applied force, which was used as the criteria for comparing piezoelectric performance. Besides piezoelectric performance, we also obtained mechanical data, including compliance (displacement divided by force) and Poisson's ratio (transverse strain divided by longitudinal strain).

For the dynamic piezoelectric study, we used the frequency analysis function in Abaqus to extract the natural frequency of the specimens. Based on the model described above, we added the density of PVDF as 1780 kg/m^3, changed the boundary conditions to be fixed on both sides with no external loading [Fig. S1(b)], and used a linear-perturbation frequency step. From this modal analysis, the first three resonance frequencies together with their deformation modes were captured.

E. Measurements

To measure the Poisson ratio of a sample, we marked the sample with an array of black dots, clamped the sample on a universal testing machine (Insight-5, MTS Systems, Eden Prairie, Minnesota), and applied tensile loading (see Supplementary Material S3 for details). The loading process was captured by a tripod-mounted DSLR camera (EOS 70D, Canon, Tokyo, Japan) and further analyzed using Photoshop (Fig. S2). The deformation ratio between transverse and longitudinal directions was calculated by counting the pixels between marked dots at different loading states. We obtained the Poisson's ratio by the ratio of the transverse and the longitudinal strains.

To measure the compliance of the specimens, we measured the force–displacement behaviors of architected piezoelectric thin films under tensile loadings using a universal testing machine (Insight-5, MTS Systems, Eden Prairie, Minnesota) and obtained the compliance by dividing displacement with force.

To measure the piezoelectric performance, we built an experiment setup as shown in Fig. S3 (see Supplementary Material S4 for details). The samples were clamped with one end connected to a load cell (LRM200, 10lbs, Futek, Irvine, California) and the other end to a shaker (APS 113, APS dynamics, San Juan Capistrano, California). The loading from the shaker was controlled to be a sine wave with frequency ranging from 10 to 150 Hz. Two electrodes were attached to the piezoelectric film and further connected with a charge amplifier (Piezo film lab amplifier, TE Connectivity, Berwyn, Pennsylvania), which converted the generated charge to the voltage signal. Both the force and the charge data were then recorded by the data acquisition system (NI-PCI 6251 and BNC-2110, National Instruments, Austin, Texas) and transmitted to computer for further analysis. As shown in Figs. S3(b) and S3(c), the force versus time and charge versus time curves were in similar shape without phase lag, indicating good time synchronization in measurements. We calculated the effective piezoelectric coefficient $\left(d_{31}^{'}\right)$ of the sample based on the applied force (F) and the generated charge (Q) in one loading cycle, using linear piezoelectric theory as Eq. (2) (see Supplementary Material S5 for details):

$$d_{31}^{'} = \frac{Qt}{FL} \quad . \tag{2}$$

To be noted here, unlike d_{33} calculation, the $d_{31}^{'}$ depends on sample's length to thickness ratio. In our experiments, all samples had the length (L) of 45 mm at the central effective area and the thickness (t) of 0.11 mm. So, we divided the charge-force ratio by $L/t = 409$ to get the effective 3-1 mode piezoelectric coefficient $\left(d_{31}^{'}\right)$. This parameter could be used as a criterion to evaluate the overall piezoelectric performance of the sample. When there is no cut, it is simply equal to material's intrinsic piezoelectric coefficient (d_{31}).

As the loading frequency is getting closer to the natural frequency of a sample, the vibration amplitude will increase causing an increase in the electrical output. We expect to observe a peak of effective piezoelectric constant $(d_{31}^{'})$ around the resonance frequency. However, since there is no resonance in tension tests, here we introduce the dynamic compressive loading for utilizing resonance features. Due to limitation of the instrument, the amplitude of the loading is very small, especially for higher frequency. The resonance feature could be beneficial for multiple applications, including ambient energy harvesting, which often falls into low frequency range and resonance could help improving the performance.

To demonstrate the application of architected piezoelectric films in ambient wind energy harvesting, we performed experiments in a wind tunnel. Figure S4 shows the testing setup for the wind energy harvesting, which can produce wind within the velocity range of 0–10 m/s. The air was driven by four computer fans (P/N PFE0381BX-000U-S99, Sunon, Kaohsiung, Taiwan) controlled by a microcontroller (Arduino UNO, Somerville, Massachusetts). The accuracy of wind velocity control was calibrated and verified by a hand-held anemometer (866B, Holdpeak, Zhuhai, China). One end of the sample was fixed on a support frame and connected to the charge amplifier. Next, wind-induced self-sustained oscillations would happen and the flapping deformation can activate the 3-1 piezoelectric mode, generating electricity. After recording the generated voltage during wind-tunnel tests, we converted them into power by considering the impedance value of 10^7 Ω and calculated the power density by considering the volume of piezoelectric materials. As the wind energy decreases with the decrease of wind velocity, we also compared the piezoelectric conversion efficiency for fair comparison, in which the generated power density is normalized by the wind power density (see Supplementary Material S6 for details).

III. RESULTS AND DISCUSSION

A. Effects of architected cuts on static piezoelectric performance

We conducted finite element method simulations and experimental measurements to investigate the effects of cut patterns on static piezoelectric performance as well as mechanical behaviors.

We first simulated static piezoelectric performance for different cut patterns. Figure 2(d) illustrates the square cut pattern samples with different cut-out ratios (0, 0.25, 0.50, and 0.75). The simulated effective piezoelectric coefficients $(d_{31}^{'})$ of the square cut pattern with different cut-out ratios are then shown in Fig. 2(f). From the simulations, we found that the $d_{31}^{'}$ is almost constant for different cut-out ratios. Similar results were observed for all other patterns (Fig. 3), suggesting that the piezoelectric performance for static tensile loadings is maintained after adding cut patterns to the film. This result suggests that we can improve the mechanical behaviors of PVDF thin films with architected cuts without negatively affecting piezoelectric performance. Then, we conducted experiments to verify the simulations by applying tensile loadings and measuring electrical outputs. As mentioned before, the loading amplitude is limited so that the sample deformation is still within the linear elastic regime. Figure 3(a) shows different cut patterns used in the measurements. We also compared the effective piezoelectric coefficient from the specimens with different cut-out ratios based on the generated charges from applied tensile loadings as shown in Fig. 3(b). The results showed similar values regardless of the cut-out ratios and showed good agreement with predictions from simulations (illustrated as dashed lines connecting data points from simulation). So, for the PVDF thin films with architected cuts that we have tested, the piezoelectric performance was independent of both cut patterns and cut-out ratios under static tensile loadings. The results provide the opportunity to modulate mechanical properties without negatively affecting piezoelectric performance. Next, to have a better understanding of the simulation and experiment results, we conducted analytical study as follows.

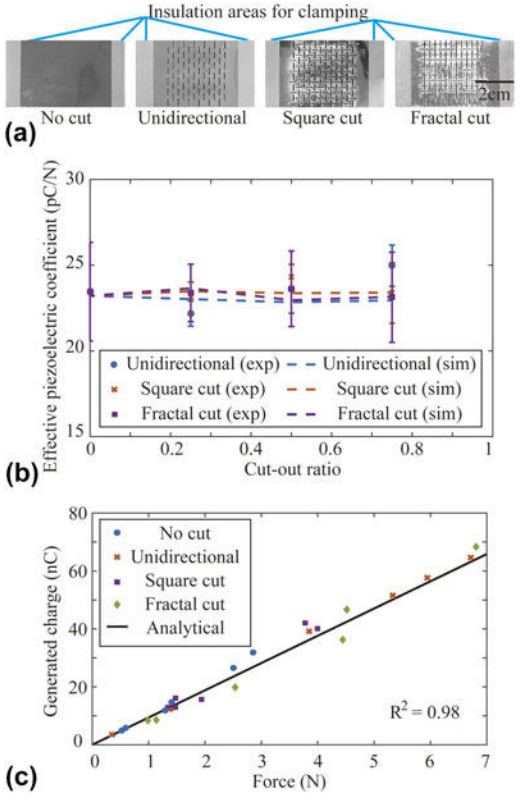

FIG. 3. (a) Samples with different cut patterns used in the study. (b) Effects of cut-out ratios on the effective piezoelectric coefficient. (c) Comparison of piezoelectric performance among different cut patterns. The points on the same slope indicate that they have the same piezoelectric performance.

Our theoretical analysis is based on the linear piezoelectric theory, where electrical output is linearly proportional to mechanical input. As a representative pattern, we considered a $L \times W \times t$ square cut film as shown in Fig. 2(c) (with m by n unit cells), where L is the length, W is the width, and t is the thickness. The unit cell length is marked as L_{unit}. Each cut has length a and width b, and the width is supposed to be much smaller than the cut length ($b \ll a < L_{\text{unit}}, L, W$) for kirigami. In each unit cell, two cuts are placed parallel with both horizontal and vertical gaps which equal to half of the unit cell length. Then, we considered the case where the film is stretched by force F in the horizontal direction. To calculate the piezoelectric performance, here we divided the film into three parts: (i) the sections without cut, (ii) the sections with horizontal cuts, and (iii) the sections with vertical cuts, as shown in Fig. 2(c). For those without cuts, the piezoelectric performance would be same with a planar piezo film. Using linear piezoelectric theory, the electrical output under this pure stretch loading could be calculated as Eq. (3)[36]:

$$\varepsilon E_3 = d_{31}\sigma_1 \quad , \tag{3}$$

where ε is the permittivity, E_3 is the electric field strength in the thickness direction, d_{31} is the piezoelectric coefficient of a material quantifying the conversion of in-plane mechanical loads to electrical energy in the direction of thickness, and $\sigma_1 = F/Wt$ is the stress in loading direction (horizontal). Therefore, the generated charge in sections without cut can be written as Eq. (4):

$$Q = CU = \varepsilon \frac{W(L - mL_{\text{unit}})}{t} E_3 t = d_{31} F \frac{(L - mL_{\text{unit}})}{t} \quad , \tag{4}$$

where U is the electric potential, equal to electric field strength multiplied by thickness; $C = \varepsilon A/t$ is the capacitance, calculated from permittivity, area, and thickness. For sections without cut, the area is $W(L - mL_{\text{unit}})$.

Similarly, for the part with horizontal cuts, the average stress inside is estimated in the form of $\sigma_1' = F/(W - 1.5nb)t$. To be noted here, the number of cuts may vary from n to $2n$ along the section, and we use the average $1.5n$, considering each situation takes a portion of 50%. This estimation should be accurate as long as $b \ll W$ (in experiments, b is 0.2 mm and W is 40.5 mm). Since we use a linear piezoelectric theory, the stress distribution has no influence on the sum of the stress, which is used to calculate the total converted electrical output. Thus, in our calculation, we can use the average stress to represent the stress state inside the target area and still get the same result. With this method, the generated charge in sections with horizontal cuts could be calculated as Eq. (5):

$$Q' = C'U = \varepsilon \frac{(W - 1.5nb)(mL_{\text{unit}} - 2mb)}{t} \times E_3 t = d_{31} F \frac{(mL_{\text{unit}} - 2mb)}{t} \quad . \tag{5}$$

Following same method, the charge generated in sections with vertical cuts could be calculated as Eq. (6):

$$Q'' = C''U = \varepsilon \frac{(W - na)2mb}{t} \times E_3 t = d_{31} F \frac{2mb}{t} \quad . \tag{6}$$

By adding Eqs. (4)–(6), we found that the total charge generation is just the same with a planar film without any cut [Eq. (7)]:

$$Q_{\text{total}} = d_{31} F \frac{L}{t} = Q_{\text{uncut}} \quad . \tag{7}$$

On the other hand, the cuts will decrease the effective area of the system, resulting in a slight decrease of the capacitance [Eq. (8)]:

$$C_{\text{total}} = \varepsilon \frac{LW - 4mnab}{t} \quad . \tag{8}$$

Then, the electric potential difference between two surfaces can be written as Eq. (9),

$$U_{\text{total}} = \frac{Q_{\text{total}}}{C_{\text{total}}} = \frac{d_{31} F}{\varepsilon} \frac{L}{LW - 4mnab} \quad , \tag{9}$$

which is slightly larger than the voltage output of the uncut sample and increases with the increasing number of cuts and the cut-out ratio [Eq. (10)]:

$$U_{\text{total}} > U_{\text{uncut}} = \frac{d_{31} F}{\varepsilon W} \quad . \tag{10}$$

However, since the cut width is considered to be much smaller than the length, i.e., $b \ll L$, the voltage difference could be negligible, if the number of cuts is small. To be noted here, this analysis is not only applicable to this specific cut pattern but also applicable to other architected cut patterns, in which we could use same dividing, averaging, and linear conversion process. Thus, we found that the static piezoelectric performance would not be influenced by adding cuts for the cases that we considered. Specifically, for samples with different cut patterns upon the same tensile loading, the amount of generated charge will remain the same, while the output voltage will slightly increase due to the decreased capacitance, which could be negligible when cut sections are infinitesimal.

We compared the charge generation upon tensile loadings for different samples as shown in Fig. 3(c). In the plot, the solid line indicates analytical results while

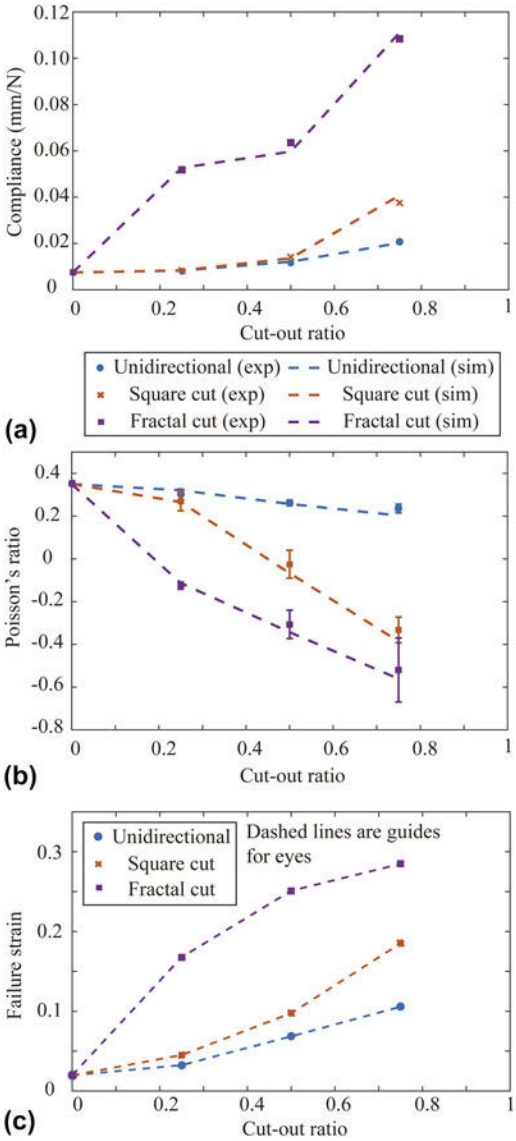

FIG. 4. Relations between cut-out ratios and (a) compliance and (b) Poisson's ratio with comparisons of simulations and experiments. (c) Failure strain for samples with different cut-out ratios and cut patterns.

symbols indicate experimental results. From the figure, we could see that all experimental points—no matter what cut patterns they have—are lying around the solid line with $R^2 = 0.98$, indicating the same effective piezoelectric coefficient.

B. Effects of architected cuts on mechanical behaviors

As piezoelectric materials are actively utilized for self-powered devices which often require customized mechanical behaviors including compliance and/or stretchability, we have investigated the effects of cut-out ratio on the mechanical behaviors. From force–displacement measurement of the architected piezoelectric thin film under tensile loadings, the compliance increased with increasing cut-out ratio and the experimental results showed good agreement with those of simulations [Fig. 4(a)]. When the cut-out ratio was 0.75, the compliance increased ~3 times for the unidirectional cut, ~6 times for the square cut, and ~14 times for the fractal cut patterns. The qualitative trend is expected from the fact that we remove materials out of specimens while it is also noticeable that removing small amount of materials can make large change in compliance.

We also measured the Poisson's ratio changes as we changed the cut-out ratios for different cut patterns. It was noted that as we increased the cut-out ratio, the sign of the Poisson's ratio changed for the case of square and fractal cut patterns, and it became more negative as we kept increasing the cut-out ratio while the Poisson's ratio remained positive for the unidirectional cut pattern within the range of the cut-out ratio we studied [Fig. 4(b)]. As the architected cut patterns have negligible solid fraction changes compared with the case having large voids, the systems allow us to study the effects of Poisson's ratio on piezoelectric performance. Then, we investigated the correlation between Poisson's ratio and the resulting piezoelectric performance by comparing results from Figs. 3(b) and 4(b). From the observation that the piezoelectric output did not change as we increased the cut-out ratios while the resulting Poisson's ratio changed from positive values through almost zero to a negative value, the Poisson's ratio does not seem to affect the piezoelectric performance in our system. This agrees well with our theoretical predictions.

In terms of stretchability, we measured the failure strain that any part of the architected thin film breaks. As shown in Fig. 4(c), the maximum strain that the architected thin film could hold increased significantly as we increased the cut-out ratio reaching about 9 times for the square cut pattern and 16 times for the fractal cut pattern with 0.75 cut-out ratio. The stretchability increased as we increased the hierarchy of the cut patterns, which is consistent with a previous study.[18] A comparison of the deformation patterns given by simulations and experiments is also illustrated in Fig. 5, comparing for both cut-out ratio changes and cut pattern changes, showing a good matching between the simulations and experiments.

C. Effects of architected cuts on dynamic piezoelectric performance

Beyond static piezoelectric performance, we also simulated and measured dynamic piezoelectric performance under compressive loadings as well as flow-induced flapping.[35] As shown in Figs. 6(a), 6(c), and 6(e), from modal analysis, we obtained the frequencies of the first three resonance modes of three cut patterns with different cut-out ratios. We found that the natural frequency

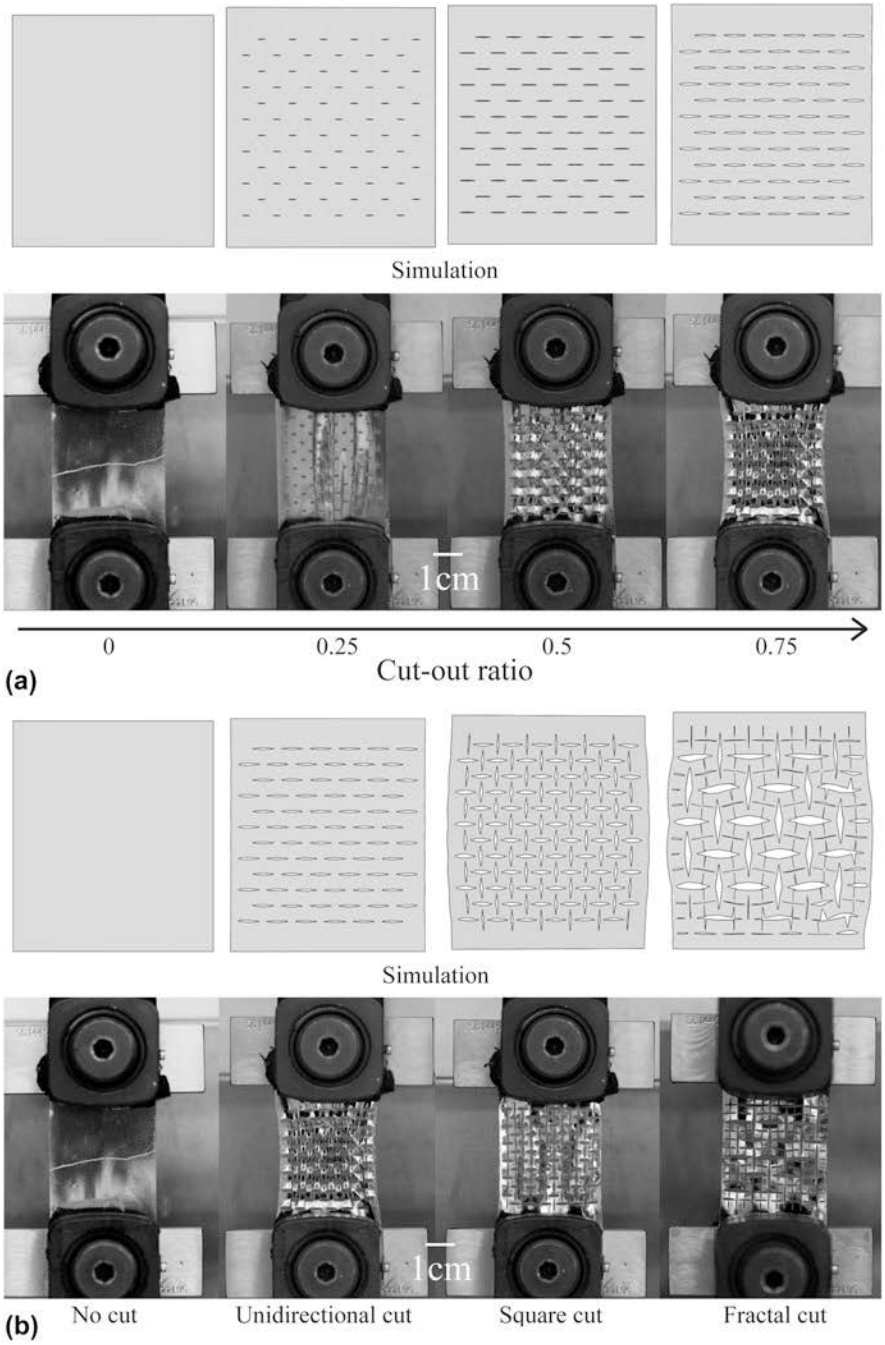

FIG. 5. Comparison of simulated deformation modes (top row) and experimental data (bottom row) for deformed samples with (a) different cut-out ratios and (b) cut patterns.

dropped significantly with the introduction of cut patterns. When there was no cut, the resonance frequency of the piezoelectric film for its first mode was ~120 Hz, while the number dropped to ~45 Hz when the cut-out ratio was 0.75. The decrease of the resonance frequency allows better usage of environmental vibrations, which are typically much smaller than 100 Hz.[34]

Figures 6(b), 6(d), and 6(f) are the experimental results showing the effects of architected cuts under dynamic compressive loadings. As the cut-out ratio increases, the piezoelectric films showed maximum ~20% increase in electrical charge outputs at a lower frequency range. With the increasing loading frequency, an overall dropping performance of the samples was observed presumably due to a combination of viscoelasticity of the material, lower loading uniformity, and insufficient sampling rate due to limitations of the instrument. However, we could still observe that the unidirectional cut sample with 0.75

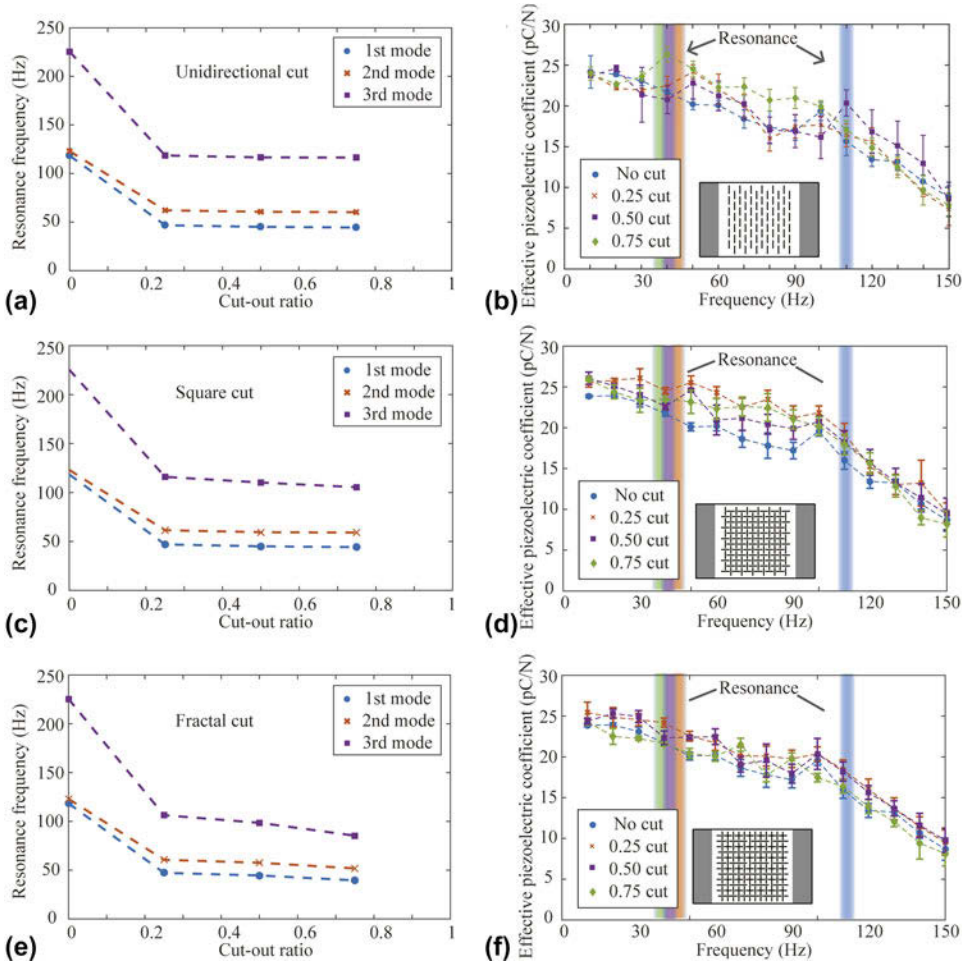

FIG. 6. Simulated resonance frequency as a function of cut-out ratio for (a) unidirectional, (c) square, and (e) fractal cut patterns. Relations between cut-out ratios and dynamic piezoelectric performance for (b) unidirectional, (d) square, and (f) fractal cut patterns.

cut-out ratio showed maximum ~25% higher effective piezoelectric coefficient around 40–50 Hz, which is at its resonance frequency range. In addition, the cut samples showed generally higher performance than the uncut samples at the higher frequency range with maximum ~30% higher performance around 110 Hz, which is the resonance frequency of the uncut sample, indicating a good versatility. As for different cut patterns, their performances were similar because they have similar resonance frequencies while the unidirectional and square cut samples showed generally higher effective piezoelectric coefficients than fractal cuts between two resonance frequencies. By designing cut patterns with specific cut-out ratio considering the range of the environmental signals, we can harvest energy that was not available due to the high resonance frequency of the original specimens. Especially, this simple method of tuning resonance frequency has advantages when geometry and mass are restricted: compared to other methods like adding weight, the cut pattern would not add mass, which is beneficial for lightweight applications and it does not require complex assembly and geometry change.

We also tested the energy harvesting performance by flow-induced flapping. Introducing cut patterns and increasing cut-out ratio could decrease the bending stiffness (as well as elastic modulus, as stated before). Thus, from Eq. (1), the film will require lower wind speed to reach self-sustained oscillation, which could generate energy. Figures 7(a), 7(c), and 7(e) show the power density change as we change the cut-out ratio. As expected, we could see that the flapping of piezoelectric materials could appear at a lower wind speed range as we increased the cut-out ratio so that we could harvest wind energy previously unable to utilize. Specifically, the uncut sample flapped in the range of 3.7–5.5 m/s, while the fractal cut pattern with the cut-out ratio of 0.75 shifted the required wind velocity range to 1.8–3.0 m/s, which is a more common wind velocity range in ambient environment. Here, the drop of power density is due to the decrease of input wind energy, which is a consequence of lower wind velocity. To make a fair comparison, we

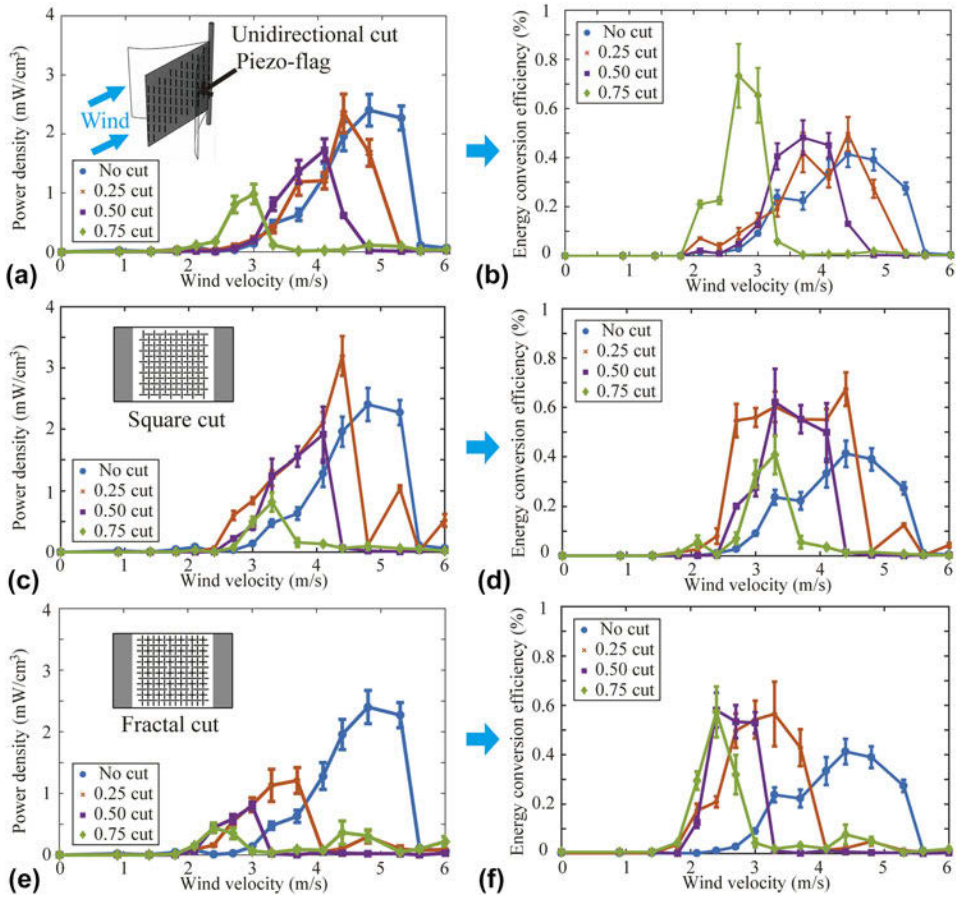

FIG. 7. Effects of changing cut-out ratio on the wind velocity range that can be utilized and the resulting power density for (a) unidirectional, (c) square, and (e) fractal cut patterns. Comparison of power conversion efficiency with the change of the cut-out ratio for (b) unidirectional, (d) square, and (f) fractal cut patterns.

normalized the generated power density by the wind power density to get the efficiency of converting wind energy into electrical energy (see Supplementary Material S6 for details). The results are plotted in Figs. 7(b), 7(d), and 7(f), in which we could observe the samples with higher cut-out ratios generally showed higher conversion efficiency in harvesting ambient wind energy. Compared with the previous study that utilized the geometry control to operate at lower wind speeds,[35] our current approach provides higher power density with the maximum two times higher value. In addition, the results also confirmed that the piezoelectric materials could have flow-induced flapping with the presence of cut patterns as they introduced very small porosities. By utilizing architected cuts, we can harvest wind energy previously unable to utilize.

IV. CONCLUSION & OUTLOOK

In this study, we systematically investigated the relationship between architected cut patterns and resulting piezoelectric and mechanical properties of piezoelectric polymer (PVDF) thin films. We conducted a combination of finite element simulations and experimental measurements to understand the effects of introducing architected cut patterns on their performance. We find that the cuts would not reduce mechanical–electrical conversion performance of piezoelectric films in static loading conditions, while they provide the possibility of introducing a variety of desirable mechanical features. For piezoelectric behaviors, we experimentally tested samples with different cut patterns and cut-out ratios and found that they had similar piezoelectric performance. In terms of mechanical behaviors, we observed that the cut samples could provide ~15 times higher compliance and stretchability, and a tunable Poisson's ratio ranging from 0.35 to −0.5 as we increased the cut-out ratio to 0.75, while maintaining the piezoelectric performance of original uncut materials. The results are supported by our simplified analytical model using linear piezoelectric theory. We also conducted dynamic loading tests coupled with numerical simulation and found that the resonance frequency of cut samples could be controlled and reduced to a frequency which is relevant to typical environmental vibrations. The samples showed maximum ~25% more piezoelectric performance at its resonance frequency,

compared with an uncut sample. Furthermore, we tested the architected thin films in wind tunnel to investigate the wind energy harvesting capability. For the same overall geometry, piezoelectric thin films with architected cuts could tune the range of wind velocity required to harvest energy and decrease it to a lower velocity range suitable for ambient environment. Moreover, it increased the energy harvesting efficiency. Our findings provide guidelines about how we can harness the architected cuts for desirable performance of piezoelectric thin films and open up possibilities for multiple engineering applications, including wearable and/or self-powered sensors and devices. Beyond the current study, the concept of architected cuts could be further applied to other functional materials.

ACKNOWLEDGMENTS

This work was supported by the start-up fund from the Whiting School of Engineering at Johns Hopkins University and the scholarship by China Scholarship Council (CSC) (J. Li). We would like to thank Dr. Shu Guo and Dr. Ugur Erturun (Johns Hopkins University) for their helpful advice.

REFERENCES

1. L. Valdevit, A.J. Jacobsen, J.R. Greer, and W.B. Carter: Protocols for the optimal design of multi-functional cellular structures: From hypersonics to micro-architected materials. *J. Am. Ceram. Soc.* **94**, 1–20 (2011).
2. R. Lakes: Foam structures with a negative Poisson's ratio. *Science* **235**, 1038–1040 (1987).
3. J.B. Choi and R.S. Lakes: Fracture toughness of re-entrant foam materials with a negative Poisson's ratio: Experiment and analysis. *Int. J. Fract.* **80**, 73–83 (1996).
4. A. Lowe and R.S. Lakes: Negative Poisson's ratio foam as seat cushion material. *Cell. Polym.* **19**, 157–167 (2000).
5. E.O. Martz, R.S. Lakes, V.K. Goel, and J.B. Park: Design of an artificial intervertebral disc exhibiting a negative Poisson's ratio. *Cell. Polym.* **24**, 127–138 (2005).
6. G.N. Greaves, A.L. Greer, R.S. Lakes, and T. Rouxel: Poisson's ratio and modern materials. *Nat. Mater.* **10**, 823–837 (2011).
7. M. Osanov and J.K. Guest: Topology optimization for architected materials design. *Annu. Rev. Mater. Res.* **46**, 211–233 (2016).
8. T.A. Schaedler and W.B. Carter: Architected cellular materials. *Annu. Rev. Mater. Res.* **46**, 187–210 (2016).
9. K. Bertoldi: Harnessing instabilities to design tunable architected cellular materials. *Annu. Rev. Mater. Res.* **47**, 51–61 (2017).
10. R.S. Lakes: Negative-Poisson's-ratio materials: Auxetic solids. *Annu. Rev. Mater. Res.* **47**, 63–81 (2017).
11. J.T.B. Overvelde, J.C. Weaver, C. Hoberman, and K. Bertoldi: Rational design of reconfigurable prismatic architected materials. *Nature* **541**, 347–352 (2017).
12. P.M. Reis, H.M. Jaeger, and M. van Hecke: Designer matter: A perspective. *Extreme Mech. Lett.* **5**, 25–29 (2015).
13. K. Bertoldi, P.M. Reis, S. Willshaw, and T. Mullin: Negative Poisson's ratio behavior induced by an elastic instability. *Adv. Mater.* **22**, 361–366 (2010).
14. K. Kim, J. Ju, and D.M. Kim: Porous materials with high negative Poisson's ratios—A mechanism based material design. *Smart Mater. Struct.* **22**, 084007 (2013).
15. K. Virk, A. Monti, T. Trehard, M. Marsh, K. Hazra, K. Boba, C.D.L. Remillat, F. Scarpa, and I.R. Farrow: SILICOMB PEEK kirigami cellular structures: Mechanical response and energy dissipation through zero and negative stiffness. *Smart Mater. Struct.* **22**, 084014 (2013).
16. M. Taylor, L. Francesconi, M. Gerendas, A. Shanian, C. Carson, and K. Bertoldi: Low porosity metallic periodic structures with negative Poisson's ratio. *Adv. Mater.* **26**, 2365–2370 (2014).
17. Y. Jiang and Y. Li: 3D printed chiral cellular solids with amplified auxetic effects due to elevated internal rotation. *Adv. Eng. Mater.* **19**, 1600609 (2017).
18. Y. Cho, J.H. Shin, A. Costa, T.A. Kim, V. Kunin, J. Li, S.Y. Lee, S. Yang, H.N. Han, I.S. Choi, and D.J. Srolovitz: Engineering the shape and structure of materials by fractal cut. *Proc. Natl. Acad. Sci. U. S. A.* **111**, 17390–17395 (2014).
19. S. Shan, S.H. Kang, J.R. Raney, P. Wang, L. Fang, F. Candido, J.A. Lewis, and K. Bertoldi: Multistable architected materials for trapping elastic strain energy. *Adv. Mater.* **27**, 4296–4301 (2015).
20. D. Restrepo, N.D. Mankame, and P.D. Zavattieri: Phase transforming cellular materials. *Extreme Mech. Lett.* **4**, 52–60 (2015).
21. J. Liu, T. Gu, S. Shan, S.H. Kang, J.C. Weaver, and K. Bertoldi: Harnessing buckling to design architected materials that exhibit effective negative swelling. *Adv. Mater.* **28**, 6619–6624 (2016).
22. S.C. Shan, S.H. Kang, P. Wang, C.Y. Qu, S. Shian, E.R. Chen, and K. Bertoldi: Harnessing multiple folding mechanisms in soft periodic structures for tunable control of elastic waves. *Adv. Funct. Mater.* **24**, 4935–4942 (2014).
23. F. Javid, P. Wang, A. Shanian, and K. Bertoldi: Architected materials with ultra-low porosity for vibration control. *Adv. Mater.* **28**, 5943–5948 (2016).
24. J.R. Raney, N. Nadkarni, C. Daraio, D.M. Kochmann, J.A. Lewis, and K. Bertoldi: Stable propagation of mechanical signals in soft media using stored elastic energy. *Proc. Natl. Acad. Sci. U. S. A.* **113**, 9722–9727 (2016).
25. S. Shan, S.H. Kang, Z. Zhao, L. Fang, and K. Bertoldi: Design of planar isotropic negative Poisson's ratio structures. *Extreme Mech. Lett.* **4**, 96–102 (2015).
26. Y.C. Tang, G.J. Lin, L. Han, S.G. Qiu, S. Yang, and J. Yin: Design of hierarchically cut hinges for highly stretchable and reconfigurable metamaterials with enhanced strength. *Adv. Mater.* **27**, 7181–7190 (2015).
27. H.A. Sodano, D.J. Inman, and G. Park: A review of power harvesting from vibration using piezoelectric materials. *Shock Vib. Digest* **36**, 197–206 (2004).
28. A. Toprak and O. Tigli: Piezoelectric energy harvesting: State-of-the-art and challenges. *Appl. Phys. Rev.* **1**, 031104 (2014).
29. A.H. Rajabi, M. Jaffe, and T.L. Arinzeh: Piezoelectric materials for tissue regeneration: A review. *Acta Biomater.* **24**, 12–23 (2015).
30. G-T. Hwang, H. Park, J-H. Lee, S. Oh, K-I. Park, M. Byun, H. Park, G. Ahn, C.K. Jeong, K. No, H. Kwon, S-G. Lee, B. Joung, and K.J. Lee: Self-powered cardiac pacemaker enabled by flexible single crystalline PMN-PT piezoelectric energy harvester. *Adv. Mater.* **26**, 4880–4887 (2014).
31. K.Y. Lee, M.K. Gupta, and S.W. Kim: Transparent flexible stretchable piezoelectric and triboelectric nanogenerators for powering portable electronics. *Nano Energy* **14**, 139–160 (2015).
32. G.T. Hwang, Y. Kim, J.H. Lee, S. Oh, C.K. Jeong, D.Y. Park, J. Ryu, H. Kwon, S.G. Lee, B. Joung, D. Kim, and K.J. Lee: Self-powered deep brain stimulation via a flexible PIMNT energy harvester. *Energ. Environ. Sci.* **8**, 2677–2684 (2015).
33. F.R. Fan, W. Tang, and Z.L. Wang: Flexible nanogenerators for energy harvesting and self-powered electronics. *Adv. Mater.* **28**, 4283–4305 (2016).

34. X. Wang, S. Niu, F. Yi, Y. Yin, C. Hao, K. Dai, Y. Zhang, Z. You, and Z.L. Wang: Harvesting ambient vibration energy over a wide frequency range for self-powered electronics. *ACS Nano* **11**, 1728–1735 (2017).
35. S. Orrego, K. Shoele, A. Ruas, K. Doran, B. Caggiano, R. Mittal, and S.H. Kang: Harvesting ambient wind energy with an inverted piezoelectric flag. *Appl. Energy* **194**, 212–222 (2017).
36. W.A. Smith: Optimizing electromechanical coupling in piezocomposites using polymers with negative Poisson's ratio. *Proc. IEEE* **1**, 661–666 (1991).
37. S. Iyer, M. Alkhader, and T.A. Venkatesh: Electromechanical behavior of auxetic piezoelectric cellular solids. *Scr. Mater.* **99**, 65–68 (2015).
38. Q. Li, Y. Kuang, and M.L. Zhu: Auxetic piezoelectric energy harvesters for increased electric power output. *AIP Adv.* **7**, 015104 (2017).
39. Z. Qi, D.K. Campbell, and H.S. Park: Atomistic simulations of tension-induced large deformation and stretchability in graphene kirigami. *Phys. Rev. B* **90**, 245437 (2014).
40. M.K. Blees, A.W. Barnard, P.A. Rose, S.P. Roberts, K.L. McGill, P.Y. Huang, A.R. Ruyack, J.W. Kevek, B. Kobrin, D.A. Muller and P.L. McEuen: Graphene kirigami. *Nature* **524**, 204–207 (2015).
41. J.N. Grima and K.E. Evans: Auxetic behavior from rotating squares. *J. Mater. Sci. Lett.* **19**, 1563–1565 (2000).

Supplementary Material

To view supplementary material for this article, please visit https://doi.org/10.1557/jmr.2018.6.